

Research Article

Sustainable Downstream Separation of Itaconic Acid Using Carbon-Based Adsorbents

Alejandra Ortíz-de-Lira,¹ Hilda Elizabeth Reynel-Ávila,^{1,2} Lizbeth Liliana Díaz-Muñoz,¹ Didilia Ileana Mendoza-Castillo,^{1,2} Tejraj M. Aminabhavi,³ Michael Badawi⁴, and Adrián Bonilla-Petriciolet¹

¹Instituto Tecnológico de Aguascalientes, 20256, Mexico

²CONACYT, 03940, Mexico

³School of Advanced Sciences, KLE Technological University, Hubballi, 580 031, Karnataka, India

⁴Université de Lorraine, Laboratoire de Physique et Chimie Théoriques LPCT UMR CNRS 7019, Vandœuvre-lès-Nancy, France

Correspondence should be addressed to Adrián Bonilla-Petriciolet; petriciolet@hotmail.com

Received 11 December 2021; Accepted 18 February 2022; Published 10 March 2022

Academic Editor: Nguyen Hai Tran

Copyright © 2022 Alejandra Ortíz-de-Lira et al. This is an open access article distributed under the Creative Commons Attribution License, which permits unrestricted use, distribution, and reproduction in any medium, provided the original work is properly cited.

Separation of itaconic acid from aqueous solution has been explored using various carbon-based adsorbents obtained from the pyrolysis and KOH activation of coconut shell biomass. The best preparation conditions to obtain a tailored adsorbent for itaconic acid purification were identified via a Taguchi experimental design, where its adsorption properties were maximized. The best activated carbon was obtained via coconut shell pyrolysis at 750 °C for 4 h plus an activation with 0.1 KOH and a final treatment at 800 °C for 2 h. This adsorbent showed an adsorption capacity of 4.31 mmol/g at 20 °C and pH 3 with a surface area of 466 m²/g. Itaconic acid separation was exothermic and pH-dependent where electrostatic forces and hydrogen bonding were the main adsorption interactions. Calculated adsorption rate constants for itaconic acid adsorption were 0.44–1.20 h⁻¹. Results of adsorbent characterization analysis indicated the presence of a crystallization of itaconic acid molecules onto the activated carbon surface where 3–4 molecules could interact to form the clusters. This organic acid was recovered from the adsorbent surface via desorption with water or ethanol, thus facilitating its final purification. The best activated carbon obtained in this study is a promising alternative to perform sustainable and energy-efficient downstream separation and purification of itaconic acid produced via fermentation.

1. Introduction

Itaconic acid (IA) is considered as a sustainable chemical with a wide range of industrial applications that includes its promising potential to replace acrylic acid and its derivatives in the manufacturing of plastics and polymeric products obtained from the petroleum [1–5]. This chemical is an unsaturated crystalline dicarboxylic acid containing double bonds having valuable properties in polymerization reactions and versatility as a block of polymer construction with ethylene dicarboxylate side chain functionality [6, 7]. Consequently, IA is a biochemical compound with a relevant and increasing commercial value [7, 8].

The traditional and most common process to obtain IA is via fermentation [1, 2]. Different strains (e.g., *Aspergillus terreus*, *Pseudozyma antartica*, and *Ustilago maydis*) and substrates (e.g., glucose, sucrose, corn starch, xylose, and sugars) have been employed during the fermentation process to obtain this acid [2, 8–10]. For instance, El-Imam and Du [11] indicated that more than 80 g/L of IA can be produced via glucose fermentation. The production of IA has been estimated around 400,000 tons/year, and its price has varied from 1.5 to 2.5 dollars/kg during over the past decades [2, 9, 10]. However, industries related to the production of chemicals from the biological sources are continuously facing challenges in terms of increments of their manufacturing costs

that are mainly associated to energy consumption and separation technologies required for the recovery and purification of the final products. These conditions have also affected the goal of a profitable and competitive production of IA [2, 12, 13], thus impacting and constraining its consumption in different industrial sectors [1, 2, 13]. Therefore, the optimization and design of high-efficiency downstream processes should contribute to resolve different technological challenges in order to achieve sustainable and economically viable production routes of IA.

One relevant aspect in this direction is the recovery and purification of IA from the fermentation broths using non-energy intensive separation processes to contribute to the reduction of its final production cost [2, 6]. In fact, there are different methods to separate IA (e.g., extraction, diafiltration, electrodialysis, and precipitation) where crystallization has been the most widely used approach, despite its well-known technical and economical disadvantages [2, 12, 14, 15]. The fermentation broths to be purified for the separation and recovery of IA are characterized by the containing biomass wastes and fermentation media residues, glucose, organic acid byproducts (e.g., malic and succinic acids), nitrates, magnesium, and calcium [2, 5]. The separation of these compounds is therefore necessary to improve the product quality and purity of IA. From the environmental protection perspective, adsorption can be an attractive separation strategy to purify IA due to its low-cost operation, reduced energy consumption, low CO₂ emissions, and the potential option to recycle and reuse the spent adsorbents already utilized as the separation media [2, 5].

To date, there are few studies focused on the separation and purification of IA via adsorption mainly using commercial adsorbents (e.g., activated carbons, zeolites, ion exchange resins, and polymeric materials) [2, 5, 14–16]. Results from literature showed that IA can be effectively separated depending on the adsorbent and process operating conditions [5, 16, 17]. Note that these studies have given a special attention to apply ion exchange resins for IA purification. Further research is needed to analyze other adsorbents and to consolidate the incorporation of adsorption as a cost-effective separation method in the supply chain of IA.

Carbon-based adsorbents prepared from lignocellulosic wastes are a promising alternative to separate IA from the fermentation broths based on the fact that they have been utilized as an effective media in different purification processes of organic molecules including IA recovery [2, 5, 18, 19]. Surface chemistry of these adsorbents can be tailored to modify their adsorption properties as well as to perform specific separation tasks [20–22]. To the best of our knowledge, a limited number of carbon-based adsorbents has been studied in the separation and purification of IA [2]. For instance, Schute et al. [5] reported the assessment of several commercial activated carbons for the separation of IA at 20 °C obtaining adsorption capacities up to 4 mmol/g to conclude that the presence of glucose did not significantly affect the separation of IA. These authors focused on the operating conditions of IA adsorption, but they did not analyze the corresponding adsorption-desorption mechanisms, which are fundamental to support the development of engineered

adsorbents with better separation properties. It is also important to highlight the existing technical gaps that should be solved with the aim of consolidating the application of carbon-based adsorbents for IA separation in fermentation broths. These gaps include optimization of adsorbent preparation conditions and tailoring of adsorbent properties to maximize the IA recovery with the aim of reducing the production costs. Also, it is necessary to understand the corresponding adsorption-desorption mechanisms along with the adsorbate-adsorbent interactions involved in the separation and recovery of IA to intensify the performance of applied adsorption processes.

The present study reports the separation of IA from aqueous solution using the carbon-based adsorbents obtained from pyrolysis of coconut shell (CS) biomass and its surface functionalization with KOH. The best preparation conditions to obtain a tailored adsorbent for IA separation were identified via Taguchi experimental design. Notice that CS is considered a lignocellulosic waste, widely produced in tropical regions worldwide [23], which is generally employed in large-scale industrial preparation of activated carbons [24]. Therefore, the application of this biomass would facilitate the transfer of the obtained results for industrial producers, thus contributing to their practical implementation and commercialization. Overall, the results of this study showed that IA separation with CS-based adsorbents can be effective and it implied a surface crystallization, which allowed the final recovery of the adsorbed IA molecules from the adsorbent surface via desorption and the corresponding reuse of this solid in subsequent separation cycles. This study thus provides new findings to promote the development of a sustainable separation and recovery of IA based on the adsorption process with carbon materials, thereby seeking to contribute for the minimization of the energy consumption, environmental impacts, and costs involved in the industrial production of this biobased chemical.

2. Methodology

2.1. Preparation and Tailoring of Coconut Shell-Based Adsorbents for the Separation of Itaconic Acid from Aqueous Solutions. CS was used as a precursor to prepare different carbon-based adsorbents via pyrolysis. This agro-industrial waste has an estimated composition of 74.1% lignin, 20.3% hemicellulose, and 0.5% cellulose, which is suitable to obtain the carbon-based materials [25]. This biomass was ground and sieved to obtain particles in the range of 0.2–0.4 mm diameter. The particles were washed, dried at 100 °C for 24 h, and used in the pyrolysis. A set of various pyrolysis conditions was tested to obtain the adsorbents with different surface properties where a L₉ Taguchi experimental design was employed to define the corresponding preparation conditions as shown in Table 1.

Firstly, the chars were obtained using a CARBOLITE Eurotherm tubular furnace where CS biomass pyrolysis was done at different conditions of temperature and dwell times under the N₂ flow rate of 400 mL/min and a heating ramp of 10°C/min. These chars were washed with deionized

TABLE 1: Taguchi L₉ experimental design used to prepare chars (CSS) and activated carbons (CSK) from the coconut shell biomass for the separation of itaconic acid from aqueous solution.

Sample No.	Pyrolysis conditions [‡]	KOH concentration, M [†]
	Temperature, °C	Dwell time, h
1	600	2
2	600	3
3	600	4
4	750	2
5	750	3
6	750	4
7	900	2
8	900	3
9	900	4

[‡]CSS adsorbents were obtained from biomass pyrolysis. [†]CSK adsorbents implied the KOH activation of CSS samples.

water and dried. Char samples were labelled as CSS, which were tested in IA adsorption to establish the basis line for data analysis. In a second stage, CSS samples were treated with different KOH concentrations (i.e., 0.1, 0.3, and 0.5 M) during 8 h at room temperature. These modified chars were further activated at 800 °C for 2 h under N₂ atmosphere. The final adsorbents were labelled as CSK and used in IA separation to compare their performance with respect to raw CSS samples. The experimental design of Table 1 allowed to analyze different conditions to prepare two types of adsorbents for IA separation from the aqueous solutions.

IA adsorption experiments for the experimental design of Table 1 were done with an adsorbent mass/IA solution volume ratio of 5 g/L, initial IA concentration of 0.23 M, and stirring speed of 120 rpm for 24 h, pH 3 at 30 °C. The pH 3 was selected for testing the performance of these adsorbents based on the fact that it is a common condition occurring in the fermentation broths during the IA production [26]. IA concentration in aqueous solutions was quantified by HPLC using a Thermo Scientific equipment with a Hypersil Gold aQ 150 mm × 4.6 mm 5 µm column. The quantification method was isocratic at a wavelength of 210 nm where the mobile phase was 1 mL/min of 0.05% phosphoric acid at 40 °C [27]. This analytical technique was employed to quantify IA concentrations in all the experiments of this study. A mass balance was utilized to analyze the IA separation by calculating the corresponding adsorption capacity (*q*, mg of adsorbed IA per g of adsorbent) (see Supporting Information (available here)).

The best conditions to prepare CS-based adsorbent for IA separation were identified using the statistical analysis of Taguchi experimental design results. The analysis was based on signal-to-noise (S/N) ratio [28], which was calculated by

$$\frac{S}{N} = -10 \log \left(\frac{1}{n_{\text{rep}}} \sum_{i=1}^{n_{\text{rep}}} \frac{1}{Rq_i^2} \right), \quad (1)$$

$$Rq_i = \left[\frac{q_{\text{CSK}}}{q_{\text{CSS}}} \right]_i, \quad (2)$$

where *n_{rep}* = 2 (i.e., experiment replicates), *q_{CSK}* and *q_{CSS}* are adsorption capacities of the CSK and CSS samples that were synthesized using the conditions mentioned in the Taguchi experimental design. The best preparation conditions to improve adsorption properties of CS-based adsorbents for IA separation were obtained via statistical analysis and maximization of S/N ratio using the software Minitab®. Kinetics and thermodynamics of IA separation, final IA recovery via desorption, and the corresponding adsorption mechanism were all studied with the best adsorbent obtained from the results of Taguchi experimental design.

2.2. Kinetics and Thermodynamics of Itaconic Acid Adsorption from Aqueous Solutions Using Coconut Shell-Based Adsorbent. The impact of pH solution on IA separation using the best adsorbent was assessed. The adsorption experiments were performed at pH 3–6 at 30 °C, IA concentration of 0.23 M, adsorbent dosage of 5 g/L, and 24 h of contact time under constant stirring. These experiments were utilized to identify the best pH value for performing the kinetics and equilibrium adsorption tests. Adsorption rate constants were determined for IA concentrations of 0.077 and 0.307 M at pH 3 (i.e., the best pH value) and 20–30 °C. Pseudo-first and pseudo-second order equations were applied to calculate the IA adsorption rate constants (see Supporting Information (available here)). Thermodynamics of IA separation was analyzed via experimental determination and data processing of the adsorption isotherms at 20–30 °C and pH 3. The equilibrium studies were done with different initial IA concentrations (0.077–0.538 M) under 24 h of constant stirring. Adsorption enthalpy (ΔH° , J/mol) was then calculated with the estimation of partition coefficient constants [29] and van't Hoff equation:

$$\ln K_{\text{ads}} = \frac{\Delta S^\circ}{R} - \frac{\Delta H^\circ}{RT}, \quad (3)$$

where ΔS° (J/mol K) is the change in entropy, *T* (K) is IA separation temperature, *K_{ads}* is adsorption equilibrium constant, and *R* (J/mol K) is the universal gas constant. The data were fitted via the linear regression of *K_{ads}* following the approach reported by Tran et al. [29].

2.3. Recovery of Itaconic Acid via Desorption from Coconut Shell-Based Adsorbent. Preliminary studies were carried out to analyze the feasibility of IA recovery from the adsorbent used as separation medium. These experiments were required to establish the effectiveness of IA desorption and adsorbent regeneration with the aim of reaching a low-energy intensive and green purification of IA from the fermentation broths. In particular, three eluents were used in IA desorption viz., deionized water at 30 and 80 °C, ethanol at 30 °C, and 0.5 M NaOH at 30 and 80 °C. These desorption agents and temperatures were selected based on the preliminary trials and results reported in other studies for IA recovery using the commercial activated carbons [2, 5]. All

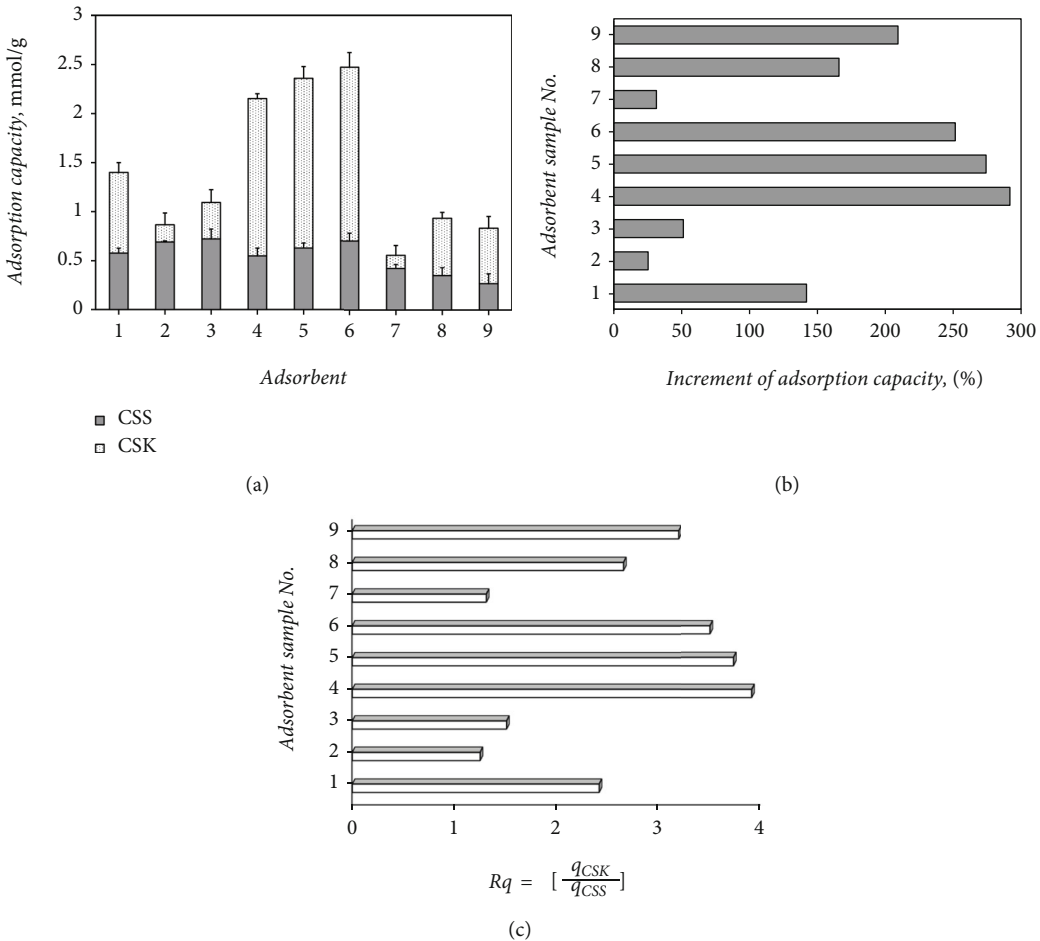


FIGURE 1: Performance of CSS and CSK adsorbents for itaconic acid separation from the aqueous solution at pH 3 and temperature of 30°C.

desorption studies were performed with a dosage of 5 g/L of IA-loaded adsorbent under constant stirring for 24 h to reach equilibrium. Notice that adsorbent samples saturated with IA at 20 °C were utilized in these experiments, and IA concentrations in the eluents were also determined using the same HPLC protocol already described for the adsorption tests to calculate the desorption rate (%):

$$\text{IA desorption (\%)} = \frac{m_{\text{rec}}}{m_{\text{ads}}} \times 100, \quad (4)$$

where m_{rec} (mg) is IA amount recovered in the desorption experiment and m_{ads} (mg) corresponds to IA amount separated from the aqueous solution with the best adsorbent used under the tested operating conditions.

2.4. Analysis of the Mechanism Involved in the Separation and Recovery of Itaconic Acid Using Coconut Shell-Based Adsorbent. Adsorption-desorption mechanism of IA separation and recovery was analyzed via physicochemical characterization of the adsorbents using the Thermo Scientific Nicolet iS10 infrared spectrophotometer. FTIR spectra were collected to characterize the surface chemistry of CSS and CSK adsorbents via KBr-adsorbent pellets at the wavenumber range of 4000-400 cm⁻¹ with 32 scans per sample. X-ray diffraction (XRD) analysis was done using Malvern-Panalytical Empyrean diffractometer equipped with a PIXel 1D detector, which was operated at 40 mA, 45 kV, the Bragg-Brentano configuration, and CuK α 1 radiation ($\lambda = 1.5406 \text{ \AA}$). The adsorbent samples with and without the loaded IA were analyzed in a step size of 0.026° in the range of 10-60° 2 θ and a scanning speed of 147 s. Phase identification was carried out with the High Score Plus software and PDF2 database. Adsorbent morphology was observed via scanning electron microscopy (SEM) using a TM 3000 scanning electron microscope (Hitachi) operated at 15 kV and working distance of 300 nm. Samples were mounted in stainless steel cylinders utilizing the double-sided carbon adhesive tape. Specific surface area of the adsorbents was determined with ASAP 2020 (Micrometrics) equipment via N₂ adsorption-desorption at -196 °C. Finally, the pH at point of zero charge (pH_{PZC}), acidity, and basicity of the adsorbents were determined as per Faria et al. [30]. Results of the adsorbent characterization were used to understand the interactions involved in IA adsorption including its recovery via the desorption. Statistical physics calculations [31] complemented the analysis of IA adsorption mechanism.

ber range of 4000-400 cm⁻¹ with 32 scans per sample. X-ray diffraction (XRD) analysis was done using Malvern-Panalytical Empyrean diffractometer equipped with a PIXel 1D detector, which was operated at 40 mA, 45 kV, the Bragg-Brentano configuration, and CuK α 1 radiation ($\lambda = 1.5406 \text{ \AA}$). The adsorbent samples with and without the loaded IA were analyzed in a step size of 0.026° in the range of 10-60° 2 θ and a scanning speed of 147 s. Phase identification was carried out with the High Score Plus software and PDF2 database. Adsorbent morphology was observed via scanning electron microscopy (SEM) using a TM 3000 scanning electron microscope (Hitachi) operated at 15 kV and working distance of 300 nm. Samples were mounted in stainless steel cylinders utilizing the double-sided carbon adhesive tape. Specific surface area of the adsorbents was determined with ASAP 2020 (Micrometrics) equipment via N₂ adsorption-desorption at -196 °C. Finally, the pH at point of zero charge (pH_{PZC}), acidity, and basicity of the adsorbents were determined as per Faria et al. [30]. Results of the adsorbent characterization were used to understand the interactions involved in IA adsorption including its recovery via the desorption. Statistical physics calculations [31] complemented the analysis of IA adsorption mechanism.

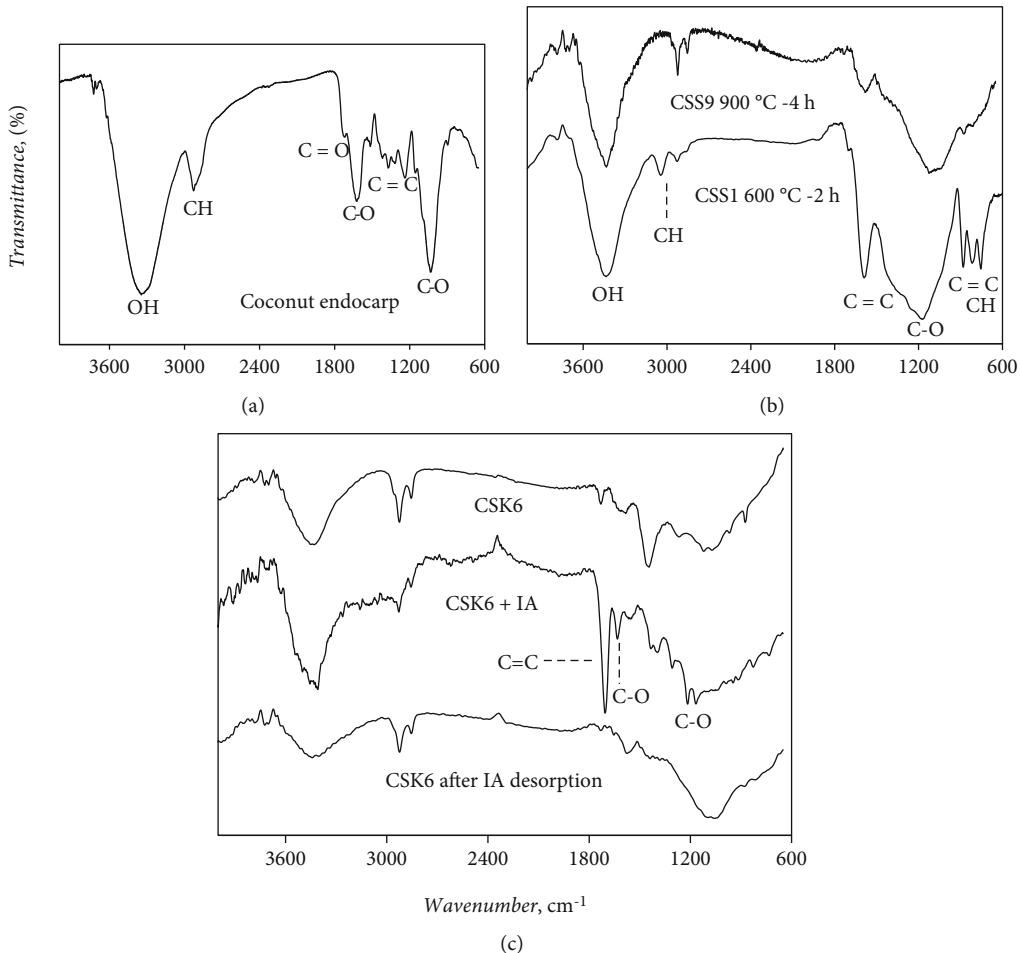


FIGURE 2: FTIR spectra of coconut shell biomass, CSS samples Nos. 1 and 9 (CSS1 and CSS9), and CSK sample No. 6 (CSK6) used in the itaconic acid adsorption.

3. Results and Discussion

3.1. Tailoring of Coconut Shell-Based Adsorbents for Itaconic Acid Separation. Figure 1 displays the performance of nine samples of CSS and CSK adsorbents prepared. Overall, the adsorbent yields ranged from 23.8 to 26.4% and IA adsorption capacities were 0.27-0.72 for CSS and 0.56-2.47 mmol/g for CSK, respectively. All the adsorbents activated with KOH outperformed the IA separation from their counterparts (i.e., CSS adsorbents), thus implying the increments of their adsorption capacities from 25 to 292% (see Figure 1(b)).

CSS adsorbent obtained from the biomass pyrolysis at 600 °C and 4h showed IA adsorption capacity of 0.72 mmol/g, while CSK adsorbent prepared from coconut shell pyrolysis at 750 °C and 4h plus KOH activation (0.1 M) achieved the highest IA separation corresponding to 2.47 mmol/g. The adsorption properties of CSS adsorbents were significantly affected by pyrolysis temperature where the lowest IA adsorption capacities were obtained at 900 °C, as shown in Figure 1. The variance analysis indicated that this biomass pyrolysis parameter showed a statistically significant effect on the IA separation (i.e., p level < 0.05), which was associated with the impact of thermal treatment

on the surface chemistry of CSS adsorbents where the functional groups were reduced as the pyrolysis temperature increased. FTIR results obtained to characterize the surface chemistry of these adsorbents indicated that functional groups of the char surface decreased with pyrolysis temperature. Figure 2 reports FTIR spectra of coconut shell biomass used as a precursor, CSS samples # 1 and 9, and the adsorbent during the IA adsorption-desorption process. The spectrum of biomass contained typical absorption bands of lignocellulosic materials as shown in Figure 2(a). The absorption bands of -OH stretching vibrations of alcohol and phenolic groups from lignin and hemicellulose were identified in the region of 3500-3100 cm⁻¹ [32-34]. The bands located around 2900-2833 and 1504-1236 cm⁻¹ were assigned to CH stretching vibrations of aliphatic groups [35-37], while the bands around 1700-1550 cm⁻¹ were associated to the conjugation of C=O, C-O, and C=C bonds that were also characteristic of cellulose and hemicellulose [34, 38]. The absorption band of C-O bond stretching vibration around 1200-1050 cm⁻¹ indicated the existence of alcohols, phenols, acids, ethers, and esters [32, 39]. SEM images of the precursor showed a nonporous irregular structure with some features typical of lignocellulosic biomasses (see Figure 3).

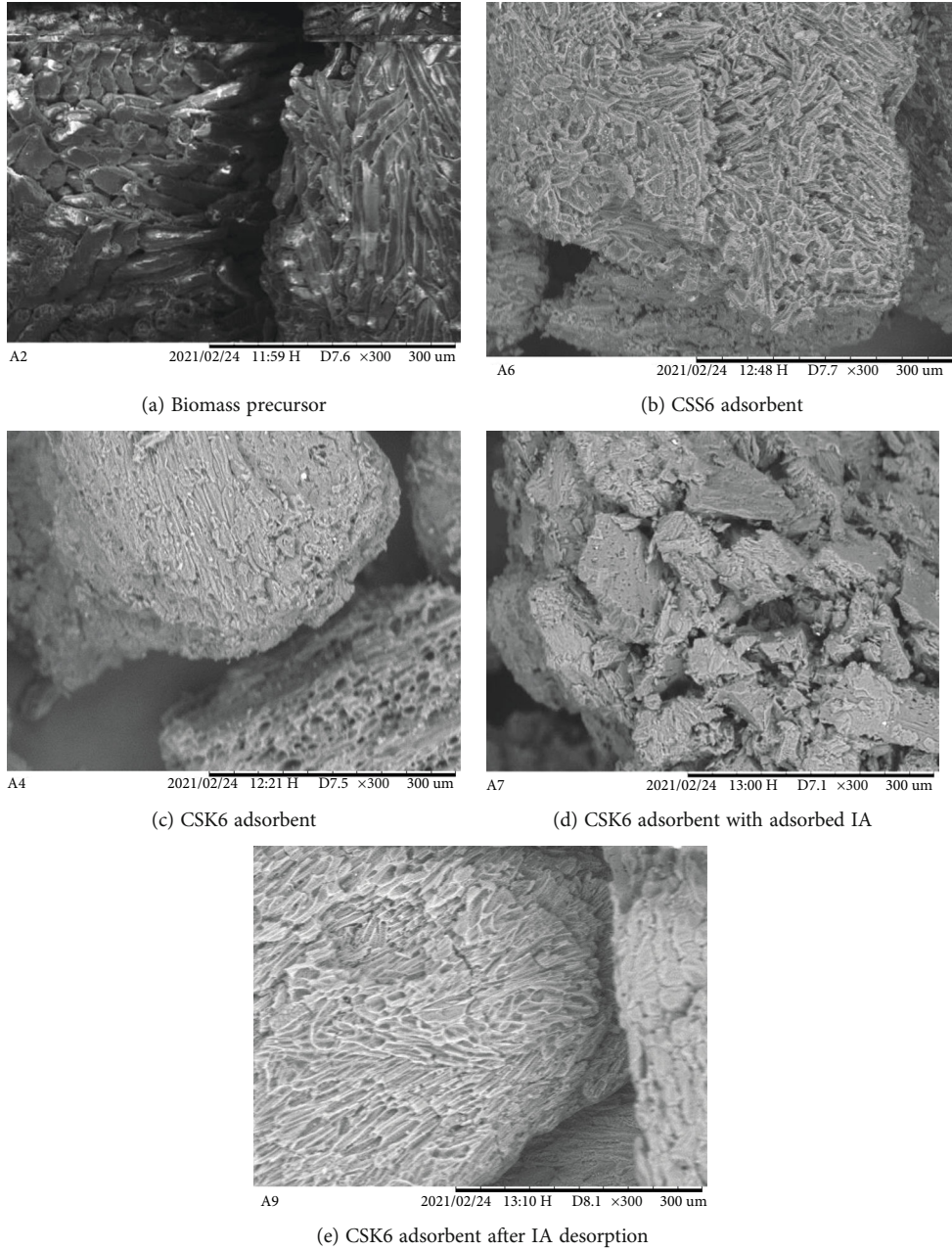


FIGURE 3: SEM images of biomass precursor and adsorbents prepared and applied in itaconic acid separation from the aqueous solution.

FTIR spectra of CSS adsorbents showed a significant reduction in the intensity of the bands associated with the carbonaceous organic compounds evidencing that pyrolysis temperature might have caused the degradation of lignin, cellulose, and hemicellulose contained in the coconut shell that was employed to prepare the adsorbents [40] as shown in Figure 2(b). Spectra of CSS1 and CSS9 samples illustrate the effect of pyrolysis conditions on the adsorbent surface functionalities. These samples were obtained with the next conditions of the Taguchi experimental design: 600 °C for 2 h and 900 °C for 4 h. A clear reduction of absorption bands was identified in the regions of 1500-1100 and 3600-3000 cm⁻¹ in comparison to the spectra of raw biomass [41]. Meanwhile, the absorption bands in the region 900-

720 cm⁻¹ related to C=C and C-H of the ring structures were formed [34, 42].

High pyrolysis temperature and dwell time generated the partial elimination of the oxygenated functionalities, which can be clearly evidenced by the reduction and/or displacement of the absorption bands at 1720 and 1164 cm⁻¹ corresponding to C=O and C-O groups, since pyrolysis conditions were more severe (Bakti and Gareso, 2018) [39]. Absorption bands at 1580 and below 900 cm⁻¹, related to C=C of aromatic rings, diminished and practically disappeared in CSS9 [40]. The bands observed at ~2950 cm⁻¹ in the spectra of CSS1 and CSS9 showed a displacement and increment of their intensity, which can be attributed to the exposure of aliphatic functional groups present in the

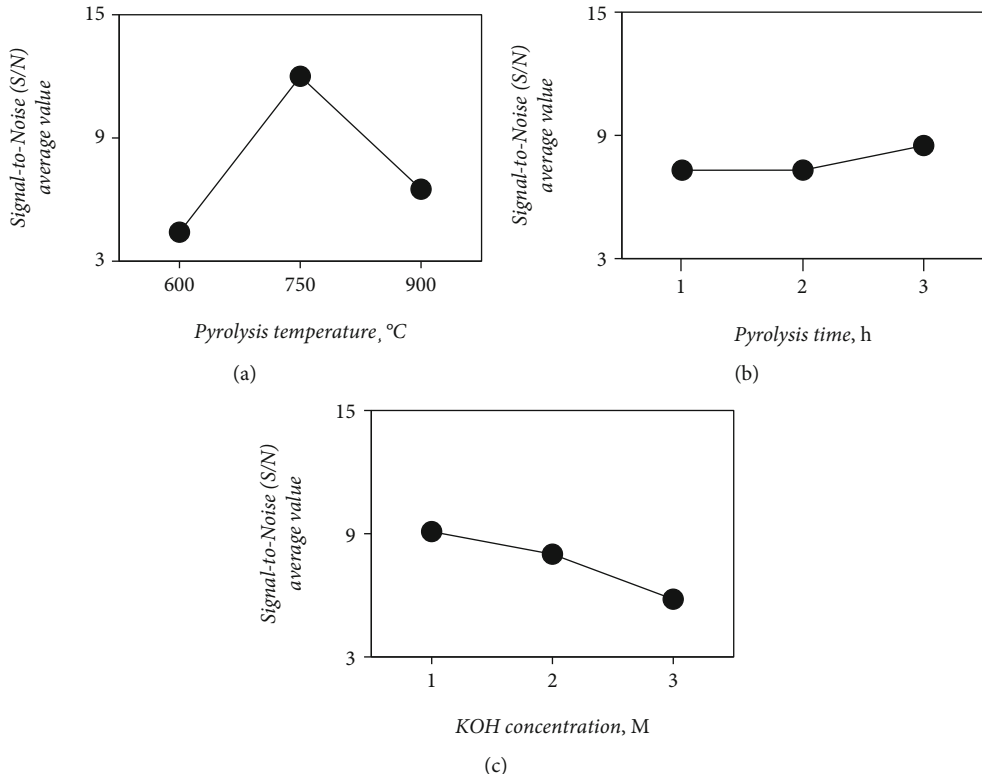


FIGURE 4: S/N analysis of the Taguchi experimental design used in the preparation of CSK for itaconic acid separation from the aqueous solution.

precursor [43, 44]. The structure of adsorbent samples showed an irregular porous form attributed to volatile matter degradation during the biomass pyrolysis [45] as shown in Figure 3. The concentration of acidic and basic functional groups of CSS adsorbents ranged from 1.91 to 1.96 mmol/g, and their pH_{PZC} was ~7.1, which was consistent with the results reported by other studies on the preparation and characterization of carbon-based adsorbents [46]. It was identified that oxygenated functional groups of these adsorbents decreased with the pyrolysis temperature, thus matching the FTIR results, and oxygenated functionalities were expected to interact with the IA molecules via H-bonding [47–49].

Figure 4 shows the S/N analysis for the preparation conditions of CSK adsorbents. Pyrolysis temperature and KOH concentration were the most relevant variables that impacted on IA adsorption properties of these adsorbents (see ANOVA results in Table S1 of Supporting Information). The pyrolysis temperature significantly affected the adsorbent surface functionalities and textural parameters, while KOH activation contributed to the porosity and formation of the oxygenated functionalities on the surface of carbon-based materials [36, 50–53]. Figure 2(c) shows FTIR spectrum of the CSK adsorbent sample No. 6. KOH functionalization caused a reduction in the intensity of the bands located around 3300–2800 and 1620 cm⁻¹ (OH, CH, and C–O groups), while the intensity of absorption band at 1100 cm⁻¹ (C=O stretching vibrations) increased [50, 54]. After the final thermal treatment, absorption bands located at 1730,

1440, and 870 cm⁻¹ increased, thus indicating the formation of oxygen groups and increment of the adsorbent aromaticity [39, 50, 53]. The concentration of basic functional groups and pH_{PZC} of CSK adsorbents increased with respect to the results obtained for CSS samples, and KOH was an effective alkaline agent to develop activated carbons with the basic surfaces [34, 50, 53, 55]. Therefore, it may be expected that this surface functionalization and activation contributed to favor the electrostatic interactions and H-bonding during the IA separation with CSK adsorbents, thus explaining their improved adsorption properties. Liang et al. [51] also concluded that KOH activation and final thermal treatment at 400–800 °C can favor the adsorbent porosity due to reaction with the functional groups on the surface of the carbon-based materials as illustrated in Figure 3, where the porous structure of CSK adsorbents was more defined due to KOH functionalization and activation. Surface area of CSK6 was 466 m²/g, which was higher than those of CSS6 samples (i.e., 353 m²/g). However, S/N analysis of Taguchi experimental design showed that IA adsorption properties of CSK adsorbents have diminished when a high KOH concentration was utilized in the activation stage. These results clearly indicated that KOH concentration should be limited to avoid negative impact on the structure and IA adsorption properties of CSK adsorbents. For instance, the surface area of sample CSK9 was 266 m²/g because of the high pyrolysis temperature and dwell time (i.e., 900 °C and 4 h) as well as KOH concentration (i.e., 0.3 M) were used in

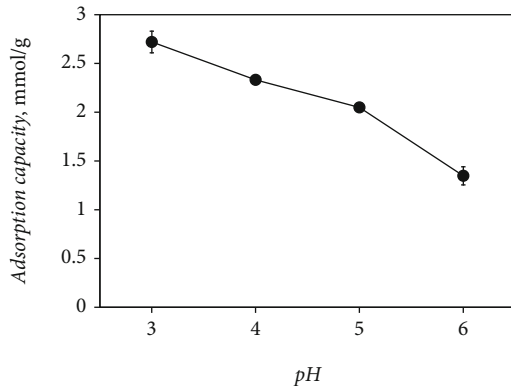


FIGURE 5: Separation of IA using CSK6 adsorbent at 30°C and different pH conditions. Initial itaconic acid concentration of 230 mmol/L.

its preparation and activation. The best conditions to prepare CSK adsorbent were identified via S/N maximization that corresponded to CSK sample # 6, i.e., coconut shell pyrolysis at 750 °C for 4 h plus activation with 0.1 M KOH and a final treatment at 800 °C for 2 h. This best adsorbent was labelled as CSK6 that was utilized to assess the kinetics and thermodynamics of IA separation. The concentrations of acidic and basic functional groups of this adsorbent were 2.31 and 3.97 mmol/g, respectively, with a $pH_{PZC} = 9.83$.

3.2. Kinetics, Thermodynamics, and Desorption for Itaconic Acid Separation Using the Best Adsorbent. The separation of IA with the sample CSK6 at different pHs displayed in Figure 5 suggested that the IA was highly pH dependent where the adsorption capacities ranged from 2.72 to 1.35 mmol/g at pH values from 3 to 6, respectively. Notice that the adsorption capacities of IA were reduced up to 50%, and that separation was favored on acidic media. Schute et al. [5] reported that IA is a dicarboxylic acid capable of being dissociated twice with the pKa values of 3.84 and 5.45, and such behavior at different pH values might be the determining factor since the polarities of the adsorbent and adsorbate could control the adsorption process. An increment in the pH caused deprotonation of IA where its polarity also increased when the molecule is fully deprotonated $pH > 7$ [5]. Notice that both neutral and IA^{1-} species were present in aqueous solution at pH 3, while only the negatively charged molecules of IA occurred at $pH > 6$, being IA^{2-} the main one. The pH might have changed the magnitude of attractive forces between CSK6 adsorbent surface and the IA molecules in aqueous media. It is noteworthy that this adsorbent was positively charged at the tested pH since $pH < pH_{PZC}$. This positive charge favored the adsorption of anionic IA species (i.e., IA^{1-} and IA^{2-}) where electrostatic attraction forces increased when the pH was reduced. These results agreed with those reported by Magalhaes et al. [14], who observed that an increment of pH decreased the IA adsorption capacity of the commercial ion exchange resins when applied in the IA separation. Similar conclusions were obtained by Schute et al. [5] while separating IA with a hypercross-linked polymer. Therefore, pH 3 was

selected as the best condition to perform the kinetic and equilibrium studies of IA separation with CSK6 adsorbent.

Figure 6 shows the kinetics of IA adsorption at pH 3, 20 and 30 °C. Overall, the IA adsorption was fast during the first 6 h, where 93-97% of IA was separated from the aqueous solution, and the maximum separation reached after 8 h when adsorption equilibrium was attained. It seems that high initial concentration of IA favored the mass transfer during adsorption, thereby accelerating its separation. The increment of solution temperature also might have reduced the IA separation up to 19.4%, thus indicating exothermic adsorption (see Figure 6). The computed kinetic parameters for the separation are shown in Table 2. The pseudo-first order kinetic equation showed the best determination coefficients ($R^2 = 0.97-0.99$) with modeling errors of ~7%. Calculated adsorption rate constants (k_1) for IA separation ranged from 0.44 to 1.20 h^{-1} under the tested operating conditions, and the kinetic model assumed the adsorption rate as proportional to the concentration of the unoccupied functional groups of the adsorbent. Pseudo-first order kinetic model has been related with the presence of physical adsorption interactions such as van der Waals and electrostatic forces besides the hydrogen bonding [56]. These intermolecular interactions can be destroyed with the increment of adsorption temperature, thereby reducing the IA separation for the adsorbent. The IA adsorption activation energy was calculated with k_1 and Arrhenius equation to obtain a value of -25.7 kJ/mol.

Experimental isotherms for the IA separation at 20 and 30 °C are reported in Figure 7. These isotherms were Langmuir-type, indicating a favorable IA separation via adsorption onto the CSK6 surface with the maximum adsorption of 4.31 mmol/g at 20 °C and 3.63 mmol/g at 30 °C, and the separation was reduced by 16% due to the increment of the temperature confirming its exothermic reaction, and results were consistent with those reported by Schute et al. [5] for the IA separation with a polymeric adsorbent where a decrease of IA adsorption was observed in the temperature range of 20–80 °C. Magalhaes et al. [14] reported exothermic IA adsorption with the ion exchange resins, and the calculated enthalpy was -13 kJ/mol, suggesting the presence of physical interactions between the adsorbent surface and the IA molecule [57, 58].

A comparison of the maximum adsorption capacities at 20 °C for CSK6 and the other adsorbents reported in literature is displayed in Table 3, where IA separation using CSK6 outperformed even the commercial activated carbons (namely, RX3 extra, SX1G, A Supra EUR, and Darco G60) reported by Schute et al. [5]. For instance, commercial adsorbents had the IA adsorption values from 0.08 to 4.1 mmol/g, in which the A Supra EUR activated carbon displayed the highest value. Similarly, Darco G60 was activated with steam, and RX3 was a cylindrical-shaped extruded activated carbon; surface areas of these commercial adsorbents ranged from 779 to 1838 m^2/g , but the highest adsorption was by the A Supra EUR. Even though these commercial activated carbons had up to threefold higher surface area than CSK6, its IA separation performance was significantly lower (i.e., <0.1 mmol/g). The commercial zeolites, viz.,

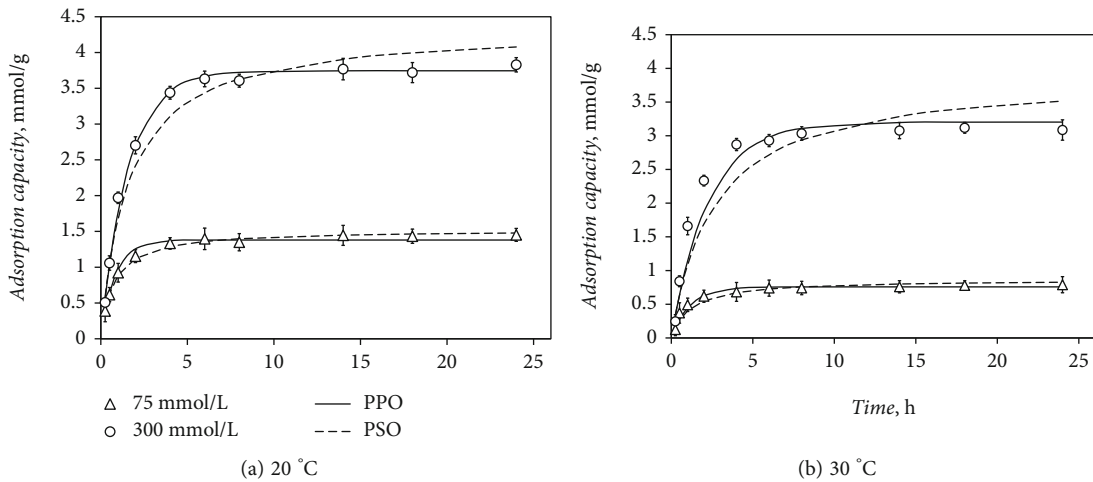


FIGURE 6: Adsorption kinetics for the separation of itaconic acid from the aqueous solution at pH 3 and modeling with the pseudo-first-order (PPO) and pseudo-second-order (PSO) equations. ○ means experimental adsorption data.

TABLE 2: Kinetic parameters for the separation of itaconic acid from the aqueous solution at pH 3 using CSK6 adsorbent.

Model	Parameters	Temperature, °C			
		20	307 mmol/L	20	307 mmol/L
Pseudo-first order	$k_1, \text{ h}^{-1}$	1.20	0.64	0.87	0.44
	$q_e, \text{ mmol/g}$	1.38	3.74	0.76	3.20
	R^2	0.98	0.99	0.97	0.97
Pseudo-second order	$k_2, \text{ g}/\text{mmol h}$	5.44×10^{-5}	8.46×10^{-6}	5.93×10^{-5}	5.80×10^{-6}
	$q_e, \text{ mmol/g}$	1.52	4.35	0.87	3.90
	R^2	0.99	0.98	0.96	0.92

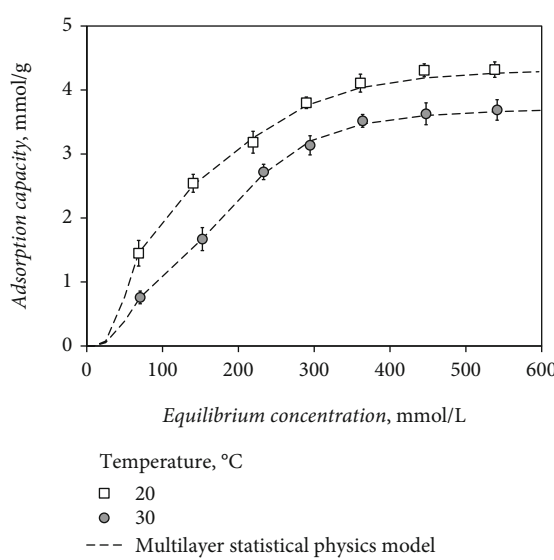


FIGURE 7: Adsorption isotherms for itaconic acid separation from aqueous solution at pH 3.

CBV 500, CBV 712, NaCZF, Na-LSX, and 13X, showed poor IA separation ranging from 0.05 to 0.83 mmol/g. Surface areas of these adsorbents were 450–815 m²/g where the zeo-

lite with the highest IA adsorption (i.e., Na-LSX, 0.83 mmol/g) had the lowest value of surface area [5]. In another case, the commercial Amberlite ion exchange resin (26 m²/g) showed the IA separation of 2.21 mmol/g, while the hypercross-linked polymer synthetized by Schute et al. [5] reached the maximum adsorption of 4.1 mmol/g, which has a surface area of 2398 m²/g. De Wever and Dennewald [16] reported the IA adsorption capacities of <0.77 mmol/g for several adsorbents including the ion exchange resins and other materials having unknown characteristics due to confidentiality issues of the company. Some of these materials were suggested as promising adsorbents for commercialization and industrial application that have outperformed the threshold value of ~0.38 mmol/g for the IA separation. From these results as well as a comparison with other adsorbents, the CSK6 adsorbent seems to be a better option that can outperform several commercial adsorbents, and CSK6 can be a good candidate for large scale application.

As per desorption data reported in Table 4, the recovery of IA ranged from 18.6 to 78.2% for the tested eluents, the highest and lowest values observed for deionized water (pH ~6) at 80 and 30 °C, respectively, while the NaOH solution showed the recovery of 33.8 and 38.5% at 30 and 80 °C, respectively, and the recovery was 28.4% for ethanol at 30 °C.

TABLE 3: Adsorption capacities of CSK6 sample and other adsorbents reported in the literature for the separation of itaconic acid [5].

Adsorbent	Adsorption capacity, mmol/g	Experimental conditions
Darco G60	1.5	
SX1G	1.7	
RX3 extra	2.5	
Amberlite	2.2	
CBV 500	0.17	0.25 mmol/L of an equimolar initial solution of itaconic acid and glucose, 0.04 g of adsorbent, 2 g of adsorbate solution, 20°C and 1 h of agitation, pH 3.7
Na-LSX	0.83	
NaCZF	0.08	
CBV 712	0.48	
13X	0.05	
Hypercross-linked polymer	4.1	0.5 mmol/L of single itaconic acid solution, 0.04 g of adsorbent, 2 g of adsorbate solution, 20°C and 1 h of agitation, pH 3.7
A Supra EUR	4.2	
This study	4.3	0.538 mmol/L of single itaconic acid solution, 0.05 g of adsorbent, 10 mL of adsorbate solution, 20°C and 24 h of agitation, pH 3

TABLE 4: Desorption of IA from CSK6 adsorbent using different eluents.

Eluent	Temperature, °C	Desorption, %
Deionized water	30	18.58 ± 1.23
	80	78.20 ± 2.18
0.5 M NaOH	30	33.81 ± 1.76
	80	38.52 ± 2.84
Ethanol	30	28.41 ± 1.62

These data confirmed an easy and feasible desorption that will facilitate obtaining the IA with a high purity. The presence of physical forces involved in the adsorption of IA molecules onto the adsorbent surface is the key to reach to high desorption rates where both temperature and pH of the desorbing agent can be important. Deionized water and ethanol are suitable for the regeneration of the carbon-based adsorbent to recover and purify IA, and the results are consistent with literature results on the recovery of IA using the ion exchange resins [5, 16]. Low-temperature desorption with ethanol is an interesting alternative to recover and purify IA. Schute et al. [5] also concluded that ethanol at 20 °C can be effective to recover and purify IA adsorbed onto the hypercross-linked polymer using the fixed-bed column, since fermentation broths contain several compounds that should be removed to purify IA. Mg and other metals can be also possible impurities while purifying IA and their separation is necessary to obtain the high-quality product. During IA separation with CSK6, the amounts of Mg and other metals adsorbed are expected to be very low, especially when the separation process is operated in acidic pH because protons in solution will inhibit and reduce the adsorption of these metallic species. Preliminary adsorption studies with CSK6 adsorbent at pH 3 showed a very low adsorption capacity of the metal ions commonly found in fermentation broths (i.e., <0.01 mmol/g). On the other hand, the recovery

of adsorbed IA is highly selective because ethanol at low temperature can minimize the desorption of heavy metals as well as other impurities loaded onto CSK6 surface. High purity IA can thus be obtained via a vacuum-based vaporization (with an aim of minimizing the energy consumption) to recover ethanol, which can be reused again during desorption.

3.3. Adsorption Mechanism in the IA Separation with the Best Coconut Shell-Based Adsorbent. FTIR spectroscopy and XRD analysis of CSK6 samples loaded with IA were utilized to study the adsorption-desorption mechanism; results are reported in Figures 2 and 8. After IA adsorption, an intense band was observed in FTIR between 1720 and 1600 cm⁻¹ that was related to stretching vibrations of C=O and C=C of IA adsorbed onto CSK6 surface [38, 59]. Absorption band at 3400 cm⁻¹ increased where this band was also related to OH group of IA. The absorption bands located at 1550, 1440, and 1100 cm⁻¹ were reduced, and changes observed for different vibration frequencies and identification of additional functional groups in FTIR spectra were attributed to adsorption of IA [38, 59]. A comparison of FTIR spectrum of CSK6 after the desorption of IA indicated a significant change in all the absorption bands. Note that the intensity of absorption bands at 3400, 1720, and 1600 cm⁻¹ decreased in the adsorbent sample obtained after the IA desorption. This is an indirect evidence of the desorption effectiveness to recover and purify IA, which can also contribute to the adsorbent regeneration and reutilization.

Figure 8 shows XRD patterns of CSK6, where peaks at 20-25 and 40-45° 2θ are characteristics of the graphitic structure of carbon-based materials with a low crystallinity [60]. After adsorption of IA, diffraction pattern indicated a significant change in the crystalline structure of the adsorbent loaded with IA. Intense peaks were identified at 19.03 and 20.60° 2θ and the peaks with less intensity were observed in the range of 23.02-40° 2θ, which were the characteristic

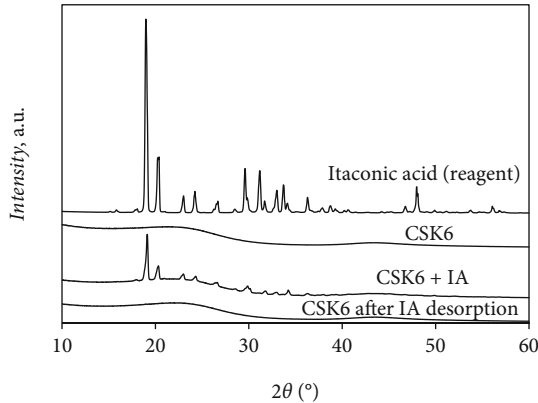


FIGURE 8: X-ray diffraction patterns of the CSK6 adsorbent with and without adsorbed IA and after its desorption.

peaks of IA structure (ICDD: 00-038-1509) [38, 61, 62]. XRD pattern of CSK6 after desorption of IA showed a significant change in the adsorbent structure where the disappearance of peaks associated with IA was clearly identified, thereby confirming that the recovery of this compound was effective and the adsorbent recuperated its original graphitic structure [39, 62]. Figure 8 displays XRD patterns of pure IA salt where it can be easily verified that the peaks identified after the adsorption were attributed to IA crystals onto the adsorbent surface, thus causing increased crystallinity [38, 59, 61]; this can be attributed to the fact that IA was crystallized onto the adsorbent surface during the separation process. In terms of morphology, CSK6 loaded with IA showed the clogged pores, attributed to IA crystals, and after the IA desorption, adsorbent showed the structure with uncovered pores, thus supporting the crystallization (see Figure 3).

EDX analysis indicated a significant increment of O content of CSK6 sample after the IA adsorption from 5 to 18%, which can be attributed to oxygenated groups of IA molecules adsorbed onto the adsorbent surface. This oxygen content was reduced almost to its original value in the adsorbent sample obtained after the IA recovery via desorption. These findings support the presence of a crystallization process during the separation of IA from the aqueous solution using CSK6 activated carbon. The occurrence of such crystallization facilitated the recovery of IA from the tested activated carbon. It is necessary to highlight that crystallization of IA onto the carbon-based porous materials has not been reported in other studies. The formation of crystalline phases onto the surface of adsorbents has been documented for other applications such as adsorption of sodium silicate and carbonate onto calcium minerals during the flotation processes [63] and adsorption of iodine compounds onto silver-exchanged mordenite to face the pollution caused by radioactive compounds in nuclear effluents [64].

A model based on statistical physics theory [31] was used to estimate some of the physicochemical parameters of IA adsorption onto CSK6 surface. This model assumed that several molecules of adsorbate (i.e., IA) can form multilayers (i.e., clusters) onto the adsorbent surface (i.e., CSK6). Details and fundaments of this model can be found in the

review of Amrhar et al. [31]. Therefore, the adsorption capacity can be defined by this model with the next equations [31].

$$q_e = n \cdot D_A \cdot \frac{F_1 + F_2 + F_3 + F_4}{G}, \quad (5)$$

$$F_1 = -\frac{2(C/C_1)^{2n}}{1 - (C/C_1)^n} + \frac{(C/C_1)^n(1 - (C/C_1)^{2n})}{(1 - (C/C_1)^n)^2}, \quad (6)$$

$$F_2 = \frac{2(C/C_1)^n(C/C_2)^n(1 - (C/C_2)^{nN_2})}{1 - (C/C_2)^n}, \quad (7)$$

$$F_3 = -N_2 \frac{(C/C_1)^n(C/C_2)^n(C/C_2)^{nN_2}}{1 - (C/C_2)^n}, \quad (8)$$

$$F_4 = \frac{(C/C_1)^n(C/C_2)^{2n}(1 - (C/C_2)^{nN_2})}{(1 - (C/C_2)^n)^2}, \quad (9)$$

$$G = \frac{(1 - (C/C_1)^{2n})}{1 - (C/C_1)^n} + \frac{(C/C_1)^n(C/C_2)^n(1 - (C/C_2)^{nN_2})}{(1 - (C/C_2)^n)^2}, \quad (10)$$

where n is the number of IA molecules that interacted and formed a cluster per functional group of CSK6 adsorbent surface, D_A (mmol/g) is the number of functional groups from the CSK6 adsorbent that was involved in IA separation, $N_T = 1 + N_2$ is the total number of layers of IA molecules formed onto CSK6 surface, and C_1 and C_2 (M) are the corresponding half-saturation concentrations of the first IA-CSK6 layer and the subsequent layers N_2 of IA-IA molecules generated during adsorption.

This model was employed to correlate IA adsorption isotherms via nonlinear regression with $R^2 > 0.99$ for both the adsorption temperatures. Modeling results indicated that a total of ~2–3 layers are formed during the adsorption of IA onto the CSK6 surface. The n values were estimated to be 3.9 at 20 °C and 3.3 at 30 °C, respectively, thus indicating that between 4 and 3 molecules of IA could interact to generate the clusters onto the CSK6 adsorbent surface during the separation process. Adsorption energies for the interactions of IA molecule-CSK6 surface ($\Delta E_{IA-CSK6}$, kJ/mol) and IA-IA molecules (ΔE_{IA-IA} , kJ/mol) were estimated as [31]

$$\Delta E_{IA-CSK6} = RT \ln \left(\frac{S_{IA}}{C_1} \right), \quad (11)$$

$$\Delta E_{IA-IA} = RT \ln \left(\frac{S_{IA}}{C_2} \right), \quad (12)$$

where S_{IA} was solubility of IA in water (mmol/L). The calculated adsorption energy for the interaction of the first adsorbate layer was ~14 kJ/mol, while the interaction energy of IA molecules during the formation of clusters on the subsequent layers was ~11 kJ/mol. These interaction energies were consistent with the presence of noncovalent forces related to the physical adsorption [31].

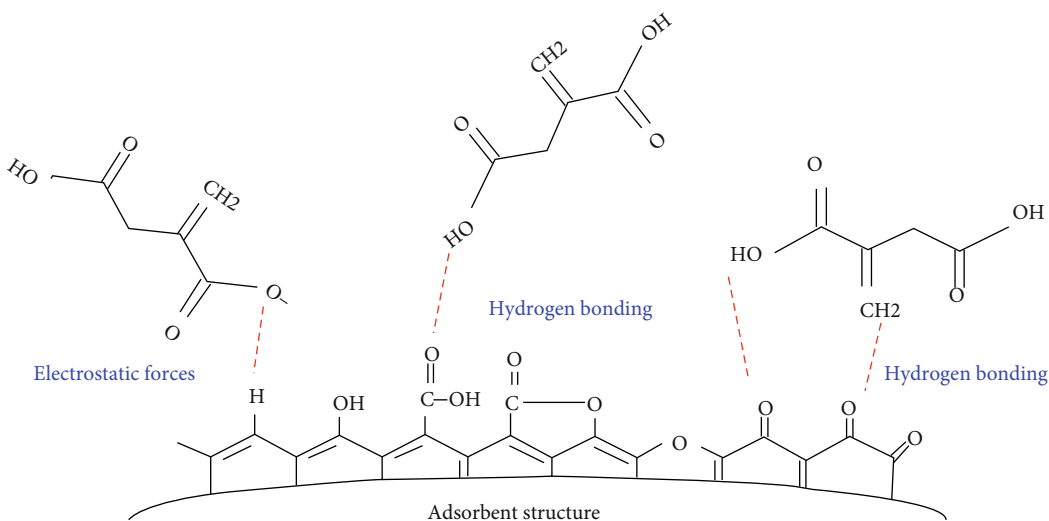


FIGURE 9: Possible adsorption mechanism for the separation of IA from aqueous solution using the best chosen coconut shell-based adsorbent.

In summary, FTIR and XRD analysis and physicochemical properties of CSK6 indicated the presence of H-bonding and electrostatic forces to be the main interactions involved in the adsorption of IA onto the adsorbent surface where the formation of IA clusters is expected. Figure 9 illustrates the proposed adsorption mechanism for the separation of IA from aqueous using the best coconut shell-based adsorbent.

4. Conclusions

The optimization of pyrolysis of coconut shell biomass and its KOH activation was effective to prepare a novel activated carbon for the low-cost and energy-efficient of itaconic acid from the aqueous solutions. This tailored adsorbent outperformed up to 10 times the threshold value of ~0.38 mmol/g required for a promising commercialization and industrial application in IA separation and purification along thus offering more advantages than those of other commercially activated carbons, zeolites, and ion-exchange resins. A high-quality itaconic acid can be obtained from the application of this adsorbent thus reducing significantly the impurities generated by Mg and other metals present in the fermentation broths. The adsorption of itaconic acid with this activated carbon implied a crystallization process that was reversible thus offering the possibility to recover of this organic acid via desorption with hot water or ethanol, and, consequently, this adsorbent can be applied in several adsorption-desorption cycles. This activated carbon represents an attractive alternative to improve the supply chain for the production of this organic acid via fermentation, thereby contributing to reduce its cost.

Data Availability

Data of this paper are available on request to the corresponding author.

Conflicts of Interest

The authors declared no potential conflicts of interest with respect to the research, authorship, and/or publication of this article.

Supplementary Materials

Supplementary information of itaconic acid properties, kinetic adsorption models, and statistical analysis results of the adsorbent preparation are reported in the supporting information file. (*Supplementary Materials*)

References

- [1] T. Klement and J. Büchs, "Itaconic acid – a biotechnological process in change," *Bioresource Technology*, vol. 135, pp. 422–431, 2013.
- [2] A. I. Magalhaes, J. C. Carvalho, J. D. C. Medina, and C. R. Soccil, "Downstream process development in biotechnological itaconic acid manufacturing," *Applied Microbiology and Biotechnology*, vol. 101, no. 1, pp. 1–12, 2017.
- [3] B. C. Saha, "Emerging biotechnologies for production of itaconic acid and its applications as a platform chemical," *Journal of Industrial Microbiology & Biotechnology*, vol. 44, no. 2, pp. 3033–3115, 2017.
- [4] B. C. Saha and G. J. Kennedy, "Phosphate limitation alleviates the inhibitory effect of manganese on itaconic acid production by *Aspergillus terreus*," *Biocatalysis and Agricultural Biotechnology*, vol. 18, article 101016, 2019.
- [5] K. Schute, C. Detoni, A. Kann, O. Jung, R. Palkovits, and M. Rose, "Separation in biorefineries by liquid phase adsorption: itaconic acid as case study," *ACS Sustainable Chemistry & Engineering*, vol. 4, no. 11, pp. 5921–5928, 2016.
- [6] S. Chellapan, D. Datta, S. Kumar, and H. Uslu, "Statistical modeling and optimization of itaconic acid reactive extraction using response surface methodology (RSM) and artificial neural network (ANN)," *Chemical Data Collections*, vol. 37, article 100806, 2022.

- [7] T. Robert and S. Friebel, "Itaconic acid – a versatile building block for renewable polyesters with enhanced functionality," *Green Chemistry*, vol. 18, no. 10, pp. 2922–2934, 2016.
- [8] R. Rebollo-Leiva, M. T. Moreira, and S. González-García, "Environmental assessment of the production of itaconic acid from wheat straw under a biorefinery approach," *Bioresource Technology*, vol. 345, article 126481, 2022.
- [9] J. C. Carvalho, A. Magalhaes, and C. R. Soccol, "Biobased itaconic acid market and research trends - is it really a promising chemical?" *Chimica Oggi*, vol. 36, pp. 56–58, 2018.
- [10] D. Gopaliya, V. Kumar, and S. K. Khare, "Recent advances in itaconic acid production from microbial cell factories," *Biocatalysis and Agricultural Biotechnology*, vol. 36, article 102130, 2021.
- [11] A. A. El-Imam and C. Du, "Fermentative itaconic acid production," *Journal of Biodiversity, Bioprospecting and Development*, vol. 1, pp. 1–15, 2014.
- [12] T. Rózsénberszki, P. Komáromy, É. Hülber-Beyer, P. Bakonyi, N. Nemestóthy, and K. Bélafi-Bakó, "Demonstration of bipolar membrane electrodialysis technique for itaconic acid recovery from real fermentation effluent of *Aspergillus terreus*," *Chemical Engineering Research and Design*, vol. 175, pp. 348–357, 2021.
- [13] N. Wierckx, G. Agrimi, P. S. Lübeck, M. G. Steiger, N. P. Mira, and P. J. Punt, "Metabolic specialization in itaconic acid production: a tale of two fungi," *Current Opinion in Biotechnology*, vol. 62, pp. 153–159, 2020.
- [14] A. I. Magalhaes, J. C. Carvalho, E. N. Ramírez, J. D. Medina, and C. R. Soccol, "Separation of itaconic acid from aqueous solution onto ion-exchange resins," *Journal of Chemical & Engineering Data*, vol. 61, no. 1, pp. 430–437, 2016.
- [15] A. I. Magalhaes, J. C. Carvalho, J. F. Thoms, J. D. Medina, and C. R. Soccol, "Techno-economic analysis of downstream processes in itaconic acid production from fermentation broth," *Journal of Cleaner Production*, vol. 206, pp. 336–348, 2019.
- [16] H. de Wever and D. Dennewald, "Screening of sorbents for recovery of succinic and itaconic acid from fermentation broths: sorption of succinic and itaconic acid from fermentation broths," *Journal of Chemical Technology and Biotechnology*, vol. 93, no. 2, pp. 385–391, 2018.
- [17] S. Gueddida, M. Badawi, H. E. Reynel-Ávila, A. Bonilla-Petriciolet, and S. Lebègue, "Selective adsorption of glucose towards itaconic acid on amorphous silica surfaces: insights from density functional theory calculations," *Journal of Molecular Liquids*, vol. 343, article 117586, 2021.
- [18] V. Dhyani and T. Bhaskar, "A comprehensive review on the pyrolysis of lignocellulosic biomass," *Renewable energy*, vol. 129, no. Part B, pp. 695–716, 2018.
- [19] P. González-García, "Activated carbon from lignocellulosic precursors: a review of the synthesis methods, characterization techniques and applications," *Renewable and Sustainable Energy Reviews*, vol. 82, Part 1, pp. 1393–1414, 2018.
- [20] A. G. Celso, G. C. Ferreira, M. C. Angelo et al., "Chemical modifications of cassava peel as adsorbent material for metals ions from wastewater," *Journal of Chemistry*, vol. 2016, Article ID 3694174, 15 pages, 2016.
- [21] S. Ding and Y. Liu, "Adsorption of CO₂ from flue gas by novel seaweed-based KOH-activated porous biochars," *Fuel*, vol. 260, article 116382, 2020.
- [22] S. Giraldo, I. Robles, A. Ramirez, E. Flórez, and N. Acelas, "Mercury removal from wastewater using agroindustrial waste adsorbents," *SN Applied Sciences*, vol. 2, no. 6, article 1029, 2020.
- [23] I. Ali, H. Bahaitam, and R. Naebulharam, "A comprehensive kinetics study of coconut shell waste pyrolysis," *Bioresource Technology*, vol. 235, pp. 1–11, 2017.
- [24] P. A. Mourão, C. Laginhas, F. Custódio, J. M. Nabais, P. J. Carrott, and M. M. Carrott, "Influence of oxidation process on the adsorption capacity of activated carbons from lignocellulosic precursors," *Fuel Processing Technology*, vol. 92, no. 2, pp. 241–246, 2011.
- [25] L. di Bitonto, H. E. Reynel-Avila, D. I. Mendoza-Castillo, A. Bonilla-Petriciolet, and C. Pastore, "Residual Mexican biomasses for bioenergy and fine chemical production: correlation between composition and specific applications," *Biomass Conversion and Biorefinery*, vol. 11, no. 2, pp. 619–631, 2021.
- [26] P. Komaromy, P. Bakonyi, A. Kucska et al., "Optimized pH and its control strategy lead to enhanced itaconic acid fermentation by *Aspergillus terreus* on glucose substrate," *Fermentation*, vol. 5, no. 2, p. 31, 2019.
- [27] G. Kaur and K. Elst, "Development of reactive extraction systems for itaconic acid: a step towards *in situ* product recovery for itaconic acid fermentation," *RSC Advances*, vol. 4, no. 85, pp. 45029–45039, 2014.
- [28] L. L. Díaz-Muñoz, A. Bonilla-Petriciolet, H. E. Reynel-Avila, and D. I. Mendoza-Castillo, "Sorption of heavy metal ions from aqueous solution using acid-treated avocado kernel seeds and its FTIR spectroscopy characterization," *Journal of Molecular Liquids*, vol. 215, pp. 555–564, 2016.
- [29] H. N. Tran, S. J. You, A. Hosseini-Bandegharaei, and H. P. Chao, "Mistakes and inconsistencies regarding adsorption of contaminants from aqueous solutions: a critical review," *Water research*, vol. 120, pp. 88–116, 2017.
- [30] P. C. Faria, J. J. Órfão, and M. F. Pereira, "Adsorption of anionic and cationic dyes on activated carbons with different surface chemistries," *Water Research*, vol. 38, no. 8, pp. 2043–2052, 2004.
- [31] O. Amrhar, L. El Gana, and M. Mobarak, "Calculation of adsorption isotherms by statistical physics models: a review," *Environmental Chemistry Letters*, vol. 19, no. 6, pp. 4519–4547, 2021.
- [32] Y. Gao, Q. Yue, B. Gao et al., "Preparation of high surface area-activated carbon from lignin of papermaking black liquor by KOH activation for Ni(II) adsorption," *Chemical Engineering Journal*, vol. 217, pp. 345–353, 2013.
- [33] M. D. Islam, M. J. Ahmed, W. A. Khanday, M. Asif, and B. H. Hameed, "Mesoporous activated coconut shell-derived hydrochar prepared via hydrothermal carbonization-NaOH activation for methylene blue adsorption," *Journal of Environmental Management*, vol. 203, Part 1, pp. 237–244, 2017.
- [34] J. Mohammed, N. S. Nasri, M. A. Zaini, U. D. Hamza, and F. N. Ani, "Adsorption of benzene and toluene onto KOH activated coconut shell based carbon treated with NH₃," *International Biodeterioration & Biodegradation*, vol. 102, pp. 245–255, 2015.
- [35] A. L. Cazetta, A. M. Vargas, E. M. Nogami et al., "NaOH-activated carbon of high surface area produced from coconut shell: kinetics and equilibrium studies from the methylene blue adsorption," *Chemical Engineering Journal*, vol. 174, no. 1, pp. 117–125, 2011.
- [36] Y. Fu, Y. Shen, Z. Zhang, X. Ge, and M. Chen, "Activated biochars derived from rice husk via one- and two-step KOH-catalyzed pyrolysis for phenol adsorption," *Science of the Total Environment*, vol. 646, pp. 1567–1577, 2019.

- [37] L. Zhang, L. T. L. Y. Liang, Q. Chen et al., "Coconut-based activated carbon fibers for efficient adsorption of various organic dyes," *RSC Advances*, vol. 8, no. 74, pp. 42280–42291, 2018.
- [38] H. Ge, T. Hua, and J. Wang, "Preparation and characterization of poly (itaconic acid)-grafted crosslinked chitosan nanoabsorbent for high uptake of Hg^{2+} and Pb^{2+} ," *International Journal of Biological Macromolecules*, vol. 95, pp. 954–961, 2017.
- [39] A. I. Bakti, P. L. Gareso, and N. Rauf, "Characterization of active carbon from coconut shell using X-ray diffraction (XRD) and SEM-EDX techniques," *Jurnal Penelitian Fisika dan Aplikasinya (JPFA)*, vol. 8, no. 2, pp. 115–122, 2018.
- [40] C. Rodriguez, M. Stollovsky, T. Hehr, Y. Rauscher, B. Rolli, and A. Kruse, "Influence of the carbonization process on activated carbon properties from lignin and lignin-rich biomasses," *ACS Sustainable Chemistry & Engineering*, vol. 5, no. 9, pp. 8222–8233, 2017.
- [41] B. Yang, Y. Liu, Q. Liang et al., "Evaluation of activated carbon synthesized by one-stage and two-stage co-pyrolysis from sludge and coconut shell," *Ecotoxicology and environmental safety*, vol. 170, pp. 722–731, 2019.
- [42] S. Krishna and C. M. Patel, "Preparation of coconut shell nanoparticles by wet-stirred media milling," *Materials Letters*, vol. 257, article 126738, 2019.
- [43] M. A. Franciski, E. C. Peres, M. Godinho et al., "Development of CO_2 activated biochar from solid wastes of a beer industry and its application for methylene blue adsorption," *Waste Management*, vol. 78, pp. 630–638, 2018.
- [44] M. Jouiad, N. Al-Nofeli, N. Khalifa, F. Benyettou, and L. F. Yousef, "Characteristics of slow pyrolysis biochars produced from Rhodes grass and fronds of edible date palm," *Journal of analytical and applied pyrolysis*, vol. 111, pp. 183–190, 2015.
- [45] O. W. Achaw and G. Afrane, "The evolution of the pore structure of coconut shells during the preparation of coconut shell-based activated carbons," *Microporous and mesoporous materials*, vol. 112, no. 1-3, pp. 284–290, 2008.
- [46] H. N. Tran, H. P. Chao, and S. J. You, "Activated carbons from golden shower upon different chemical activation methods: synthesis and characterizations," *Adsorption Science & Technology*, vol. 36, no. 1-2, pp. 95–113, 2018.
- [47] Y. Huang, W. Zhang, M. Bai, and X. Huang, "One-pot fabrication of magnetic fluorinated carbon nanotubes adsorbent for efficient extraction of perfluoroalkyl carboxylic acids and perfluoroalkyl sulfonic acids in environmental water samples," *Chemical Engineering Journal*, vol. 380, article 122392, 2020.
- [48] J. P. Silva, A. L. Costa, S. S. Chiaro, B. E. Delgado, M. A. de Figuiredo, and L. F. Senna, "Carboxylic acid removal from model petroleum fractions by a commercial clay adsorbent," *Fuel Processing Technology*, vol. 112, pp. 57–63, 2013.
- [49] L. Zhang, J. Guo, Z. Xie, B. Li, and S. Liu, "Micro-mechanism of improving low-rank coal flotation by using carboxylic acid collector: a DFT calculation and MD simulation study," *Colloids and Surfaces A: Physicochemical and Engineering Aspects*, vol. 622, article 126696, 2021.
- [50] W. Chen, M. Gong, K. Li et al., "Insight into KOH activation mechanism during biomass pyrolysis: chemical reactions between O-containing groups and KOH," *Applied Energy*, vol. 278, article 115730, 2020.
- [51] Q. Liang, Y. Liu, M. Chen et al., "Optimized preparation of activated carbon from coconut shell and municipal sludge," *Materials Chemistry and Physics*, vol. 241, article 122327, 2020.
- [52] O. Oginni, K. Singh, G. Oporto, B. Dawson-Andoh, L. McDonald, and E. Sabolsky, "Influence of one-step and two-step KOH activation on activated carbon characteristics," *Bioresource Technology Reports*, vol. 7, article 100266, 2019.
- [53] D. G. Zavarize, "Insights on preparation and characteristics of KOH-doped carbons derived from an abundant agroindustrial waste in Brazil: Amazon acai berry seeds," *Bioresource Technology Reports*, vol. 13, article 100611, 2021.
- [54] E. Yagmur, Y. Gokce, S. Tekin, N. I. Semerci, and Z. Aktas, "Characteristics and comparison of activated carbons prepared from oleaster (*Elaeagnus angustifolia* L.) fruit using KOH and $ZnCl_2$," *Fuel*, vol. 267, article 117232, 2020.
- [55] E. M. Mistar, T. Alfatah, and M. D. Supardan, "Synthesis and characterization of activated carbon from *Bambusa vulgaris striata* using two-step KOH activation," *Journal of Materials Research and Technology*, vol. 9, no. 3, pp. 6278–6286, 2020.
- [56] S. K. Jain, N. A. Shakil, A. Dutta, J. Kumar, and M. K. Saini, "Sorption kinetics and isotherm modelling of imidacloprid on bentonite and organobentonites," *Journal of Environmental Science and Health. Part. B*, vol. 52, pp. 1–12, 2017.
- [57] H. N. Bhatti, N. Akhtar, and N. Saleem, "Adsorptive Removal of Methylene Blue by Low-Cost *Citrus sinensis* Bagasse: Equilibrium, Kinetic and Thermodynamic Characterization," *Arabian Journal for Science and Engineering*, vol. 37, no. 1, pp. 9–18, 2012.
- [58] N. Pérez, J. González, and L. A. Delgado, "Estudio termodinámico del proceso de adsorción de iones de ni y v por parte de ligninas precipitadas del licor negro kraft," *Revista Latinoamericana de Metalurgia y Materiales*, vol. 31, pp. 168–191, 2011.
- [59] R. Abbasi, A. Nodehi, and M. Atai, "Synthesis of poly(acrylic-co-itaconic acid) through precipitation photopolymerization for glass-ionomer cements: Characterization and properties of the cements," *Dental Materials*, vol. 36, no. 6, pp. e169–e183, 2020.
- [60] H. P. Khalil, M. Jawaaid, P. Firoozian, U. Rashid, A. Islam, and H. M. Akil, "Activated carbon from various agricultural wastes by chemical activation with KOH: preparation and characterization," *Journal of Biobased Materials and Bioenergy*, vol. 7, no. 6, pp. 708–714, 2013.
- [61] D. Pathania, C. Verma, P. Negi et al., "Novel nanohydrogel based on itaconic acid grafted tragacanth gum for controlled release of ampicillin," *Carbohydrate polymers*, vol. 196, pp. 262–271, 2018.
- [62] D. M. Patil, G. A. Phalak, and S. T. Mhaske, "Design and synthesis of bio-based UV curable PU acrylate resin from itaconic acid for coating applications," *Designed Monomers and Polymers*, vol. 20, no. 1, pp. 269–282, 2017.
- [63] Y. Foucaud, M. Badawi, L. O. Filippov, O. Barres, I. V. Filippova, and S. Lebegue, "Synergistic adsorptions of Na_2CO_3 and Na_2SiO_3 on calcium minerals revealed by spectroscopic and ab initio molecular dynamics studies," *Chemical Science*, vol. 10, no. 43, pp. 9928–9940, 2019.
- [64] T. Bucko, S. Chibani, J. F. Paul, L. Cantrel, and M. Badawi, "Dissociative iodomethane adsorption on Ag-MOR and the formation of AgI clusters: an ab initio molecular dynamics study," *Physical Chemistry Chemical Physics*, vol. 19, no. 40, pp. 27530–27543, 2017.